

Nanobiomechanical behavior of Fe3O4@SiO2 and Fe3O4@SiO2-NH2 nanoparticles over HeLa cells interfaces

Juan Carlos C Camacho-Fernández, Génesis Karendash González Quijano, Childerick Severac, Etienne Dague, Véronique Gigoux, Jaime Santoyo-Salazar, Adrian Martinez-Rivas

▶ **To cite this version:**

Juan Carlos C Camacho-Fernández, Génesis Karendash González Quijano, Childerick Severac, Etienne Dague, Véronique Gigoux, et al.. Nanobiomechanical behavior of Fe3O4@SiO2 and Fe3O4@SiO2-NH2 nanoparticles over HeLa cells interfaces. Nanotechnology, 2021, 32 (38), pp.385702. 10.1088/1361-6528/ac0a13 . hal-03260468

HAL Id: hal-03260468
https://laas.hal.science/hal-03260468

Submitted on 15 Jun 2021

HAL is a multi-disciplinary open access archive for the deposit and dissemination of scientific research documents, whether they are published or not. The documents may come from teaching and research institutions in France or abroad, or from public or private research centers.

L'archive ouverte pluridisciplinaire **HAL**, est destinée au dépôt et à la diffusion de documents scientifiques de niveau recherche, publiés ou non, émanant des établissements d'enseignement et de recherche français ou étrangers, des laboratoires publics ou privés.

Nanobiomechanical behavior of Fe_3O_4@SiO_2 and Fe_3O_4@SiO_2-NH_2 nanoparticles over HeLa cells membranes

J.C. Camacho-Fernández[1], G.K. González-Quijano[2], C. Séverac[3], E. Dague[4], V. Gigoux[5], J. Santoyo-Salazar[6] and A. Martinez-Rivas[7].

[1]ENCB-Instituto Politécnico Nacional (IPN), Av. Wilfrido Massieu, Unidad Adolfo López Mateos, 07738, Mexico City, Mexico.
[2]CONACYT-CNMN-IPN, Av. Luis Enrique Erro s/n, Nueva Industrial Vallejo, 07738, Mexico City, Mexico.
[3]ITAV-CNRS, Université de Toulouse, CNRS, Toulouse, France.
[4]LAAS-CNRS, Université de Toulouse, CNRS, Toulouse, France.
[5]INSA, Université de Toulouse, CNRS, Toulouse, France.
[6] Departamento de Física, Centro de Investigación y de Estudios Avanzados, CINVESTAV, Av. IPN 2508, Zacatenco, 07360, Mexico.
[7] CIC-Instituto Politécnico Nacional, Av. Juan de Dios Bátiz, Nueva Industrial Vallejo, 07738, Mexico city, Mexico
Corresponding author: nanobiomex@hotmail.com, sjimmyster@gmail.com

Abstract

In this work, the behavior of HeLa cells incubated with Magnetic Nanoparticles (MNPs) and exposed to an Alternating Magnetic Field (AMF) was tested. The membrane mechanical properties, tested by AFM, showed significant modification when the cells were exposed to both MNPs and AMF. The magnetite nanoparticles (Fe_3O_4) were synthesized by a coprecipitation method, encapsulated with silica (SiO_2): Fe_3O_4@SiO_2 and functionalized with amino groups (NH_2): Fe_3O_4@SiO_2-NH_2 by sonochemical processing at a reaction time bellow 2 h. The characterization of the 3 types of MNPs was done by X-ray diffraction (XRD), FT-IR spectroscopy, X-ray photoelectron spectroscopy (XPS) and high resolution transmission electron microscopy (HR-TEM), to define the lattice, composition and morphology of the nanocore-shells. The HeLa cells were treated with two types of MNPs: Fe_3O_4@SiO_2 and Fe_3O_4@SiO_2-NH_2, at a temperature of 37 ° C. The mechanical analysis, performed through Atomic Force Microscopy (AFM) indentations, provided the Young modulus and stiffness of the cells. Control HeLa cells (reference), without MNPs and without AMF, presented values of 7.1 ± 5.6 kPa for the Young modulus and 4.9 ± 0.4 nN/µm for the stiffness. The statistical analysis with $p<0.001$ showed significant differences between the reference and the cells exposed to MNPS and AMF. Interestingly, the treatment showing the most significant difference was AMF applied to Fe_3O_4@SiO_2-NH_2 exposed HeLa cells, with YM and stiffness mean values of respectively 1.4 ± 0.6 kPa and 2.5 ± 0.4 nN/µm.

Keywords: Magnetic nanocore-shells, HeLa cells, alternating magnetic fields, AFM analysis, biomechanics.

---

1. Introduction

Magnetic nanoparticles (MNPs) are widely used in biomedicine due to their potential applications in magnetic separation, or as therapeutic drug, in radio frequency and as an agent enhancing contrast in magnetic resonance imaging [1]. Magnetite (Fe_3O_4) is the most studied kind of MNPs, mainly used in magnetic resonance imaging (MRI) [2], drug delivery systems [3],

biosensors [4], clinical assays [5] and hyperthermia treatments [6]. MNPs can be synthetized by different techniques, including thermal decomposition [7], hydrothermal [8], sol-gel process [9] and more recently, green synthesis [10]. However, coprecipitation method is still used for by research groups because of its simplicity, low cost and high yield [11].

Coprecipitation synthesis of Fe_3O_4 MNPs is based on the precipitation of Fe^{3+} and Fe^{2+} ions with a molar ratio 2:1 mixed in an alkaline media according to the reaction: $2Fe^{3+} + Fe^{2+} + 8OH^- \rightarrow Fe_3O_4 + 4H_2O$. Magnetite is easily oxydated in the air, transforming it in another iron oxide called maghemite (γ-Fe_2O_3). Maghemite, unfrotuantely have a lower magnetic susceptibility [12]. To avoid the oxidation and the loss of magnetite properties, the magnetite nanoparticles are thus, often covered with either inorganic or polymeric layers, such as gold, silver, polyethylene glycol (PEG) or chitosan. In addition to avoiding the oxidation of the magnetite these coatings confer to MNPs additional features. For example, one of the most widely used inorganic material for coating is silicon dioxide (SiO_2), commonly named silica. This coating has very interesting properties: it is thermally stable [13], optical response [14], high functionality [15], and moreover, it is biocompatible [3]. That is why SiO_2 became the preferred material for biomedical applications[16]. Magnetite coating by silica is normally performed by the Stöber process through hydrolysis and polycondensation of the tetraethyl orthosilicate (TEOS) in alcohol media, water, and ammonium [17]. The reaction allows to obtain nanocore-shells of the kind Fe_3O_4@SiO_2. Mechanical stirring in the Stöber encapsulation, has been reported with times of 16 h [18], and up to 24 h [19]. Nevertheless, Morel et al. 2008, reported that Stöber encapsulation of Fe_3O_4 assisted by sonochemical treatment could be performed in just 1 to 3 h [20].

Silica surfaces are easily functionalized. The amine functional group (-NH_2) for instance is used for its easy coupling with linkers such as 1-ethyl-3-(3-dimethylaminopropyl)carbodiimide (EDC), n-hydroxysuccinimide (NHS) or biomolecules with hydroxide (-OH) or thiol (-SH) groups [21]. This binding capability allows research to obtain the conjugation of amino acids, proteins, enzymes, antibodies, among others, increasing the functionality and specificity within the biomedical area. Additionally, it has been reported that amine functionalization over silica NPs decreases the toxicity levels compared with the non-functionalized silica NPs [22, 23].

MNPs have been studied to develop the therapy called magnetic hyperthermia. MNPs within a high frequency alternating magnetic fields (AMF) actually heat, causing cell death in the heated zone. When the MNPs are subjected to an AMF, the magnetic energy is transformed into heat on the grounds of the osciallation of their magnetic domains. This osciallation induces a temperature increase, sufficient to simulate apoptosis or necrosis processes in cancer cells. The cytotoxic effect due to hyperthermia was described by Hildebrandt el al. 2002 [28]This strategy has been tested against cancer cells from prostate [24], breast [25], pancreas [26] or in cell lines of cervical cancer like the HeLa [27]. However, several studies show that AMF can induce cell death without perceptible temperature rise. Indeed, Villanueva et al. 2010, showed that HeLa cells, incubated with a concentration of 0.5 mg/ml of manganese nanoparticles coated with SiO_2, exposed to AMF (15 mT, 100 kHz), presented cellular damage leading to cell death, while the temperature reached during AMF treatment did not exceed 37.5 °C [29]. Clerc et al. 2018 [30] and Sanchez et al. 2014 [31] experimented AMF (40 mT, 275 kHz) on different cell lines, incubated with targeted MNPs, and also showed the induction of cell death without detectable temperature rise in the bulk. Using fluorescent thermometers, they demonstrated a significant temperature increase of the MNPs which were internalized in the cells lisosomes. They concluded that cell death is initiated in the lysosomes, consecutively to a local hyperthermia and through a lysosomal pathway [30]. These latter studies, validated the induction of cell death by the combined effect of the MNPs and AMF exposure, at temperatures below 43 °C. Moreover, they differ from standard magnetic hyperthermia whereby tumor eradication is achieved with large doses of MNPs which cause a temperature elevation of the whole tumor [6].

Recently, Atomic Force Microscopy (AFM) has been widely used in cancer research, due to its ability to conduct studies and analysis of both the morphology and the mechanical properties of cells and tissues ~~membranes~~. The main cell properties that have been investigated with AFM are cell height, roughness, nuclear morphology, stiffness and Young's modulus [32]. These studies, taken altogether, show that mechanical properties could be used to decipher between normal cells or tissues and canceorus cells/tissues. They all suffer from their statistical shortage, which is intrinsic to AFM studies, performed cell by cell by an highly trained experimentator. This limitation prevent us to further consider AFM as a diagnoistic tool and researchs in the direction of automation are therefore of great interest (ICI CITER NOUS, mais AUSSI LES AUTRES AUTOMATISATIONS, cf papier Sergio) ~~[33, 34]~~.

In the context of Pelling et al. 2009 reported a decrease in Young's modulus during the early stages of apoptosis [35]. This is attributed to the cytoskeleton structures disorganization and the actin filaments reduction [36]. Young's module is

determined through non-linear adjustment with the Hertz model applied to the nanoindentation process, meanwhile stiffness is adjusted by a linear equation of the slope. Both are related to each other, and bring physical features in the materials about their deformation ratio [37]. Other experiments have been performed to analyze the effect of MNPs on the mechanical properties of non-cancer cells. Mao et al. 2015, found an increment in the Young´s modulus of bovine articular chondrocytes. The reported values were 1.82, 3.02, 3.60 and 3.80 kPa because of the increment of the iron oxide nanoparticles concentration of 0, 5, 10, 20 and 50 µg/ml, respectively [38]. Currently, cells with MNPs have been incubated for 24 h before applying AMF in order to study the effects produced by the MNPs inside of the cells [10, 39].

The present work pushes the understanding of magnetic hyperthermia on plasma membrane behavior, by addressing its mechanical properties including Young's modulus and stiffness. A fast silica encapsulation and amino functionalization over Fe_3O_4 nanoparticles were conducted, using sonochemical treatment with a reaction time of 2 h. HeLa cells were incubated with these MNPs for 30 min allowing their interaction with plasma membrane. The mechanical analysis, were performed in an AFM, following or not magnetic hyperthermia exposure. conclusion sur effet nanos seules? Et effet hyperthermie

These experiments suggest the viability of Fe_3O_4@SiO_2-HN_2 such as therapy agents against HeLa cells.

2. Materials and method

2.1 Materials

Iron (II) chloride tetrahydrate ($FeCl_2 \cdot 4H_2O$) was purchased from J. T, Baker. Iron (III) chloride hexahydrate ($FeCl_3 \cdot 6H_2O$) ACS reagent 97%, tetramethylammonium hydroxide ($N(CH_3)_4OH$) 25 wt. % in H_2O and (3-aminopropyl) triethoxysilane (APTES) 99% were acquired from Sigma-Aldrich. Ammonium hydroxide (NH_4OH) 30-32% and hydrochloric acid (HCl) min 37% were purchased from Vetec. Tetraethyl orthosilicate (TEOS) reagent grade 98% was from Aldrich. Distilled water and ethanol 99%. HeLa cells were cultured in complete medium Dulbecco's modified Eagle medium (DMEM) with GlutaMAX containing 10% fetal bovine serum (FBS). 100 IU/ml penicillin/streptomycin in a humidified atmosphere at 95% air and 5% CO_2 at 37 °C. (Life Technologies).

2.2 Synthesis of Fe_3O_4 MNPs

Magnetite was synthesized by coprecipitation method using the concentrations reported by Doui et al. 2006 [40]. 54 ml of distilled water with 10 ml of HCl was prepared. 6.96 g of $FeCl_3$ salts were dissolved in 25 ml of HCl solution and 2.52 g of $FeCl_2$ in 6.25 ml of HCl solution for 1 h. Then, 10 ml of $FeCl_3$ and 2.5 ml of $FeCl_2$ were mixed and stirred at 500 rpm in a round-bottom three-necked flask heated up at 70 °C and bubbled with argon for 15 min. Once homogenized, 21 ml of $N(CH_3)_4OH$ were added to the solution keeping the stirring for 40 min. The final substance was black color, meaning the successful synthesis of magnetite. A magnet was put under the flask to precipitate the magnetite and the waste reaction was removed by decanting. MNPs were washed 5 times with ethanol and distilled water until reaching a neutral pH 7. At the end, Fe_3O_4 nanoparticles were dispersed in distilled water and lyophilized for 36 h to obtain the Fe_3O_4 powders.

2.3 Silica encapsulation: Fe_3O_4@SiO_2 MNPs

Encapsulation was carried out via the Stöber method with sonochemical assistance as reported by Morel et al. 2008 [20] with some modifications. First, 13 mg of Fe_3O_4 powders were sonicated and dispersed in 30 ml of ethanol for 30 min. Subsequently, 700 µl of NH_4OH were mixed with 9.3 ml of distilled water for 5 min. The resultant solution was added to the reaction and was sonicated for 30 min. At last, 400 µl of TEOS was added in the reaction and was sonicated for 2 h. All the sonication reaction was performed in a Branson B1510 Ultrasonics, at 40 kHz of frequency. Core-shells MNPs were centrifuged and washed two times with ethanol/distilled water (50%), and finally 3 more times with ethanol. Fe_3O_4@SiO_2 were dispersed in ethanol and dried at room temperature. For the HeLa cell treatments, 1 mg of MNPs were dispersed in 100 µl of distilled water.

2.4 Amine functionalization: $Fe_3O_4@SiO_2$ MNPs

9 mg of $Fe_3O_4@SiO_2$ powders were sonicated in 15 ml of ethanol for 30 min. A mixture of 3 ml of distilled water and 150 µl of NH_4OH was aggregated and sonicated for 30 min. 100 µl of APTES was added, the sonication applied for 2 h. Amine functionalized MNPs were centrifuged and washed two times with ethanol/distilled water (50%), and finally 3 more times with ethanol. $Fe_3O_4@SiO_2$-HN_2 were dispersed in ethanol and dried at room temperature.

2.5 Characterization of MNPs

Crystallographic structure of the three types of MNPs were analyzed by X-ray diffraction (XRD) using a Rigaku Smart Lab diffractometer with a Cu K_α radiation wavelength of 1.5424 Å. Angle range of 2θ was of 20° to 70° at a scanning rate of 0.02°. FT-IR spectra were recorded from 1800 to 400 cm^{-1} in a NICOLET 6700 device. The X-ray photoelectron spectrometer (XPS) spectra were performed by Thermo Fisher Scientific Company with a monochromatic Al kα X-ray source from 760 to 0 eV.

High-resolution transmission electron microscopy (HR-TEM) images of $Fe_3O_4@SiO_2$ were obtained by a JEOL ARM-200F operating at 200 kV. Samples were previously dispersed in ethanol and deposited on formvar carbon copper grids by dropping.

2.6 Cell culture and magnetic treatments in HeLa cells

The magnetic field (AC) device is a Fives Celes-Lautenback commercial generator. Cell treatment by high frequency alternating magnetic field (AMF) was performed as follows. HeLa cells were cultured for 24 h, prior to the experimentation in Petri dishes with a density of $75x10^3$ cells/dish with 2 ml of complete medium in a controlled atmosphere of 37 °C with 5% CO_2. Treated cells were incubated with $Fe_3O_4@SiO_2$ or $Fe_3O_4@SiO_2$-NH_2 at a concentration of 100 µg/ml for 30 min at 37 °C in a complete medium. Incubation medium was withdrawn and cells were rinsed twice with incubation medium and then incubated with complete medium. Petri dishes were placed inside the coil and exposed to AMF (278.5 kHz, 40 mT) for 30 min or 1 h. The temperature of the Petri dishes was maintained at 37.0 ± 0.2 °C and monitored with Reflex-Neoptix temperature sensor. A Petri dish without MNPs and without applying AMF was used as reference. Three Petri dishes were pipetted with 20 µl of $Fe_3O_4@SiO_2$, separately two Petri dishes with 20 µl of $Fe_3O_4@SiO_2$-NH_2, and another Petri dish was left without MNPs. All Petri dishes were incubated for 30 min at 37 °C in an incubator. Then, the three conditions of the Petri dishes were exposed to AMF for 1 h. Another Petri dish with $Fe_3O_4@SiO_2$ was exposed for 30 min to determine the best time of exposure to the magnetic field. Finally, two Petri dishes with $Fe_3O_4@SiO_2$ and $Fe_3O_4@SiO_2$-NH_2, were maintained without exposition of the AMF. After treatments with AMF, all cell cultures were supplemented with 10 µl of antibiotic (penicillin/streptomycin) and incubated for 24 h in a controlled atmosphere of 37 °C with 5% CO_2.

2.7 Mechanical analysis by atomic force microscopy (AFM)

All the samples were analyzed by an AFM (JPK model Nanowizard III) coupled with a Zeiss Axio Observer precision engine (S/N SM-01-0017) and a Zeiss Axiovert 200M inverted microscope. From each experiment, some cells were selected and analyzed to determinate the Young's modulus and stiffness. The AFM was used to perform force spectroscopy, and especially in the force mapping mode. 10x10 (100 indentations) matrix of force curves were recorded in an area of 3x3 μm^2. The maximum applied force was set to 1 nN, the Z length to 6 µm scanned in 1.2 s. We used commercial conical indenter (Bruker MLCT) with a nominal spring constant of 0.01 N/m. The Sensitivity and spring constant of each cantilever were calibrated by measuring respectively the slope of the approach curve on a glass slide and the thermal noise method. The force maps obtained were processed in JPKSPM Data Processing software. Each force curve was extracted, processed to calculate the indentation and adjusted to the Hertz model to determine the Young's modulus. We used the Hertz model for conic indenter expressed in the following equation: $F = \frac{2E}{\pi(1-\upsilon^2)}\delta^2 \tan(\alpha)$.

Where F is the force, E is the Young´s modulus, υ is the Poisson's ratio (0.5), δ is the probe penetration into the cell and α is the half cone angle (17.5°).

2.8 Statistical analysis

Statistical comparison among reference and treatments was performed by one-way ANOVA analysis with Tukey test using $p<0.001$ to determine significant differences. Analysis were conducted in IBM SPSS Statistics software version 25.

3. Results and discussion.

3.1 XRD characterization

The diffractograms relating to Fe_3O_4, $Fe_3O_4@SiO_2$ and $Fe_3O_4@SiO_2$-NH_2 are display in Fig.1. The diffraction patterns of magnetite were compared with the File (JCPDS-65-3107). Space group of $Fd\bar{3}m$ (227), lattice parameter of a = 8.396 Å and a cubic inverse structure was determined for the three samples. The peaks for Fe_3O_4 are located at 30.25°, 35.63°, 43.31°, 53.74°, 57.22° and 62.84° [16, 41]. The absence of peaks displacements in 2θ allows confirming that the coating and the functionalization on the magnetite nanoparticles do not alter its crystalline structure. Nevertheless, changes in the intensity are present because of the scattering effect from amorphous silica and amine group layers.

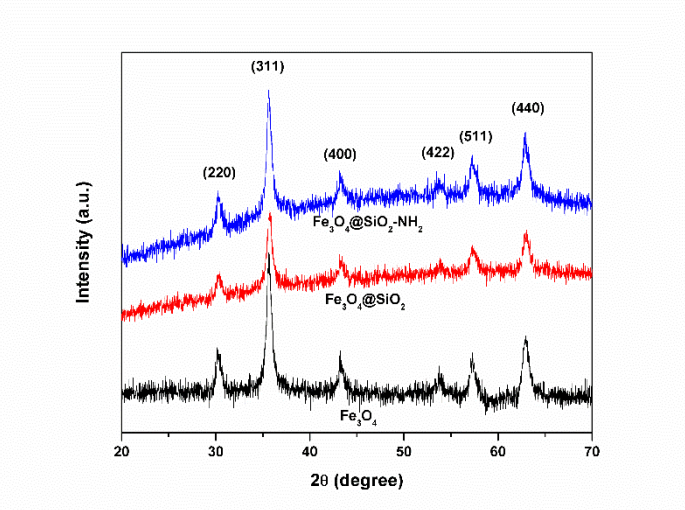


Fig. 1 XRD patterns of Fe_3O_4 (black), $Fe_3O_4@SiO_2$ (red) and $Fe_3O_4@SiO_2$-NH_2 (blue).

3.2 FT-IR spectrum

The FT-IR spectrum is depicted in Fig. 2. The peak at 570 cm^{-1} illustrates the Fe-O vibration due to the magnetite phase [42], and it is the principal visible peak in the Fe_3O_4 IR. In the two remaining spectra, other well defined peak at 1070 cm^{-1} is observed and corresponds to Si-O-Si asymmetric stretching vibration while C-Si-O vibration is provided at 460 cm^{-1} by the silica coating [43]. The weak peak located at 945 cm^{-1} is related to the stretching vibration of Si-O-Fe [44]. Regarding the amine-modified MNPs, the peak at 1630 cm^{-1} is assigned to the bending and stretching vibration of the aliphatic amine N-H [45] and the peak at 800 cm^{-1} is due to the bending vibration of N-H which is overlapped by the stretching band of Si-OH vibration [46].

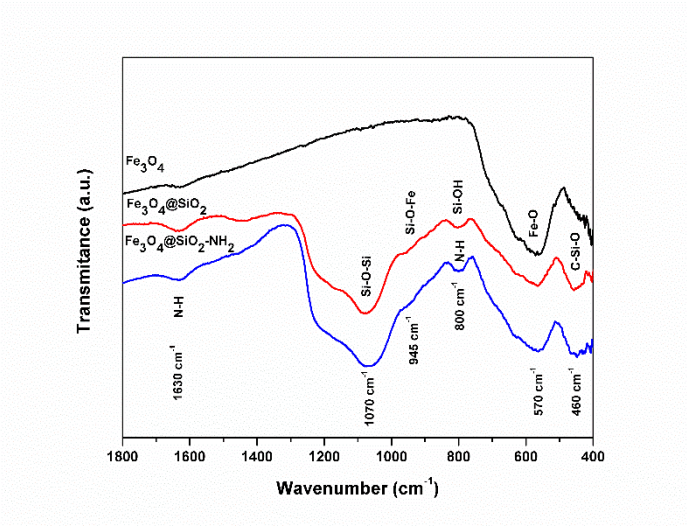


Fig. 2 FT-IR spectrum of Fe_3O_4 (black), Fe_3O_4@SiO_2 (red) and Fe_3O_4@SiO_2-NH_2 (blue).

3.3 XPS

The XPS spectrum of Fe_3O_4 has peaks at 720 eV and 710 eV which are associated to Fe 2p bindings, while 95 eV is due to Fe 3s, 60 eV is related to Fe 3p bindings. Fe peaks in Fe_3O_4@SiO_2 almost disappeared, but Si 2s and Si 2p appear at 155 and 100 eV respectively, due the silica covering [47]. After the amination with APTES, a peak of N 1s is observed at 400 eV indicating the proper functionalization over silica shells [48]. In the three samples, peaks at 530 eV for O 1s and 285 eV for C 1s were observed.

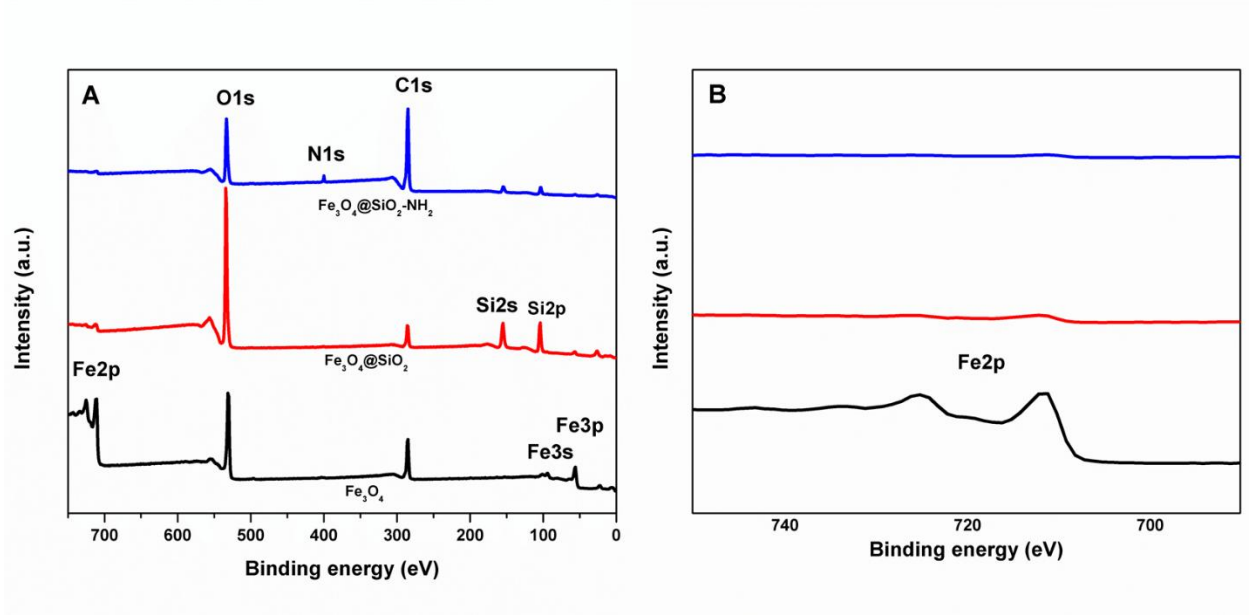


Fig. 3 XPS analysis of Fe_3O_4 (black), Fe_3O_4@SiO_2 (red) and Fe_3O_4@SiO_2-NH_2 (blue). A) 760-0 eV region, B) Fe 2p region.

3.4 HR-TEM

The silica encapsulation around Fe_3O_4 MNPs of 10.45 nm in average was successfully obtained. The layer SiO_2 thickness over Fe3O4 MNPs was around 5.85 nm (Fig. 4A). In addition, the high-resolution analysis, permit us to observe the amorphous surface of the silica shells, and determine the interplanar space of the magnetite as 4.86 Å at [111] (Fig. 4B).

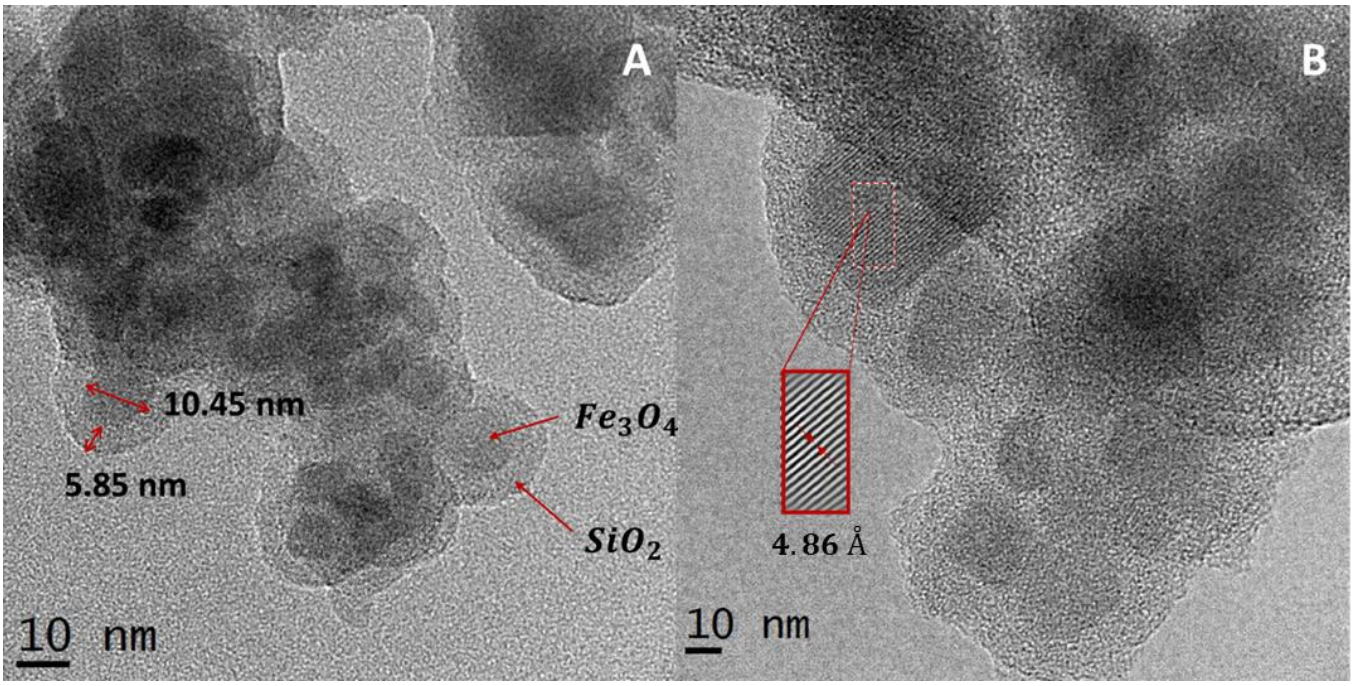


Fig. 4 HR-TEM images of Fe_3O_4@SiO_2. A) Magnetic cores were measured with an average size of 10.45 nm and silica shells with 5.85 nm of thickness. B) Interplanar space of magnetite obtained with HR-TEM at 4.86 Å.

3.5 Mechanical properties of HeLa cells analyzed by Atomic force microscopy

Force spectroscopy according to a matrix of 10x10 force curves was conducted on control and treated cells. Figure 5 presents a typical approach and retraction cycle with the elasticity and stiffness maps, as recorded on a control cell. For each condition we analyzed at least XXX cells from XXX different cultures and XXX treatments. The elasticity values (Young modulus) and stifness values are the ???(average) and ??? (standard deivation) of XXX force curves. In order to compare the conditions (control and different treatments) we decided to perform an ANOVA test. This statistical analysis demonstrated significant differences in Young's modulus and stiffness with $p < 0.001$, among the reference and all treatments. It suggests that each treatment corresponding to incubation with non-functionalized or amino-functionalized MNPs, AMF exposure or MNPs incubation plus AMF exposure, have influenced the nanomechanical properties of the HeLa cells. ~~membranes~~. The Young's modulus for the HeLa reference, corresponding to cells devoid of MNPs in absence of AMF application was 7.07 ± 5.56 kPa (Fig. 6A). The first comparison parameter is the use of the two types of MNPs without AMF induction. The experiment with Fe_3O_4@SiO_2 has minimum decrease of 37.48% as an average value of 4.42 ± 2.14 kPa was maintained. However, the experiment with Fe_3O_4@SiO_2-NH_2 had an average value of 1.97 ± 1.24 kPa, which implied a decrement of 72.13%. These experiments indicated that there is an effect caused by the interaction between cells and the different types of MNPs, which directly affects the elastic properties of the cells. This effect is amplified in the amino-functionalized MNPs, suggesting a higher interaction between the cell membranes and the aminated MNPs. The other experiments were done over HeLa cells exposed to AMF at 40 mT and 278.5 kHz. The AMF application decreased the Young's modulus of cells without MNPs by of 64.35%, with an average value of 2.52 ± 1.16 kPa, whereas it decreased by 43.28% with 4.01 ± 1.96 kPa and 67.18% with a value of 2.32 ± 1.97 kPa of cells incubated with Fe_3O_4@SiO_2 and exposed to AMF for 0.5 and 1 h respectively. The minimum value for Young's modulus was obtained for Fe_3O_4@SiO_2-NH_2 MNPs with 1 h of exposure to AMF, which reached a decrement of 80.62% with 1.37 ± 0.61 kPa. Hence, AMF treatment has an effect over the HeLa cell interface decreasing their elasticity values and making them more susceptible to deformation. Besides, AMF treatment had higher decrements when it was combined with the MNPs, obtaining the highest decrease with the amino-functionalized MNPs.

The stiffness was also evaluated by comparing the average value of the treated samples against the value obtained from the reference sample corresponding to 4.91 ± 0.42 nN/µm (Fig. 6B). The first comparison was made between MNPs without AMF. The functionalized MNPs (Fe_3O_4@SiO_2-NH_2) had a difference of 33.80% (3.25 ± 0.39 nN/µm), while the MNPs of Fe_3O_4@SiO_2 gave a difference of 22.40% (3.81 ± 0.66 nN/µm). Similar to Young's modulus, stiffness was reduced depending on the type of MNPs used. The exposure to AMF without MNPs had a decrease of 32.17% and maintained an average value of 3.33 ± 0.55 nN/µm. Stiffness in HeLa cells exposed at AMF and at different times exhibited a significant difference ($p<0.001$) between 0.5 and 1 h, although their mean values were not distant. For 0.5 h exposure values obtained were 3.48 ± 1.26 nN/µm and for the 1 h exposure 3.59 ± 0.68 nN/µm, with decrements of 29.12% and 26.88% respectively. Finally, the use of Fe_3O_4@SiO_2-NH_2 during 1 h of exposure to the AMF, presented the largest decrement with 2.52 ± 0.37 nN/µm, which represents a difference of 48.67% with respect to the reference. For the stiffness, AMF treatment had a minimum value compared with the combined treatment with AMF and silica MNPs. It turned out that heat produced by the AMF in the cells made their membranes softer.

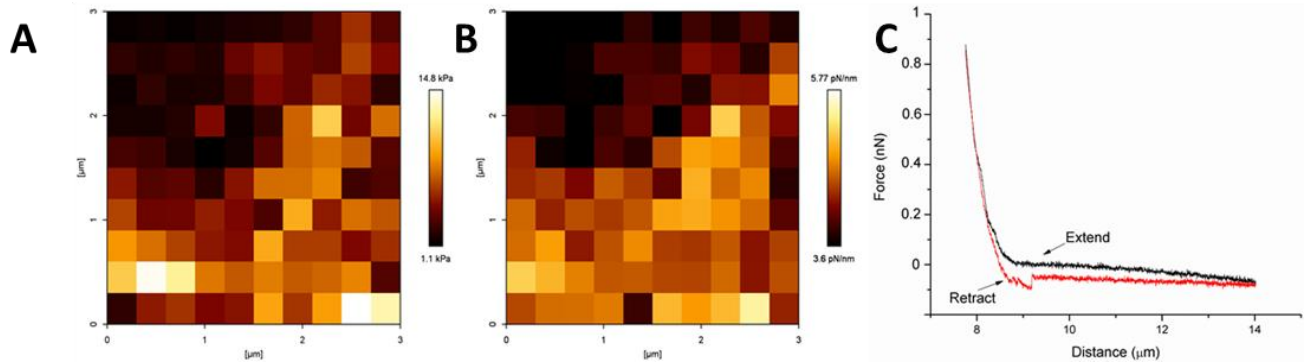


Fig. 5 Elasticity and stifness maps recorded on a control cell. A) corresponds to a typical force curve showing the approach curve (black) and the retraction in red. Single FC are recorded according to a matrix of 10x10, in 3x3µm^2 area. The young modulus is calculated for each curve and plotted as an elasticity map (B). The stiffness, which is basically the slope of the retraction force curve is plotted as a stifness map in C. ~~Images of force curves after data processing done in a Reference cell with matrix size of 10x10, in 3x3 µm area. A) corresponds to Young´s modulus and B) image to stiffness. Young´s modulus was adjusted with the extend curve, and stiffness was adjusted with the retract curve in C).~~

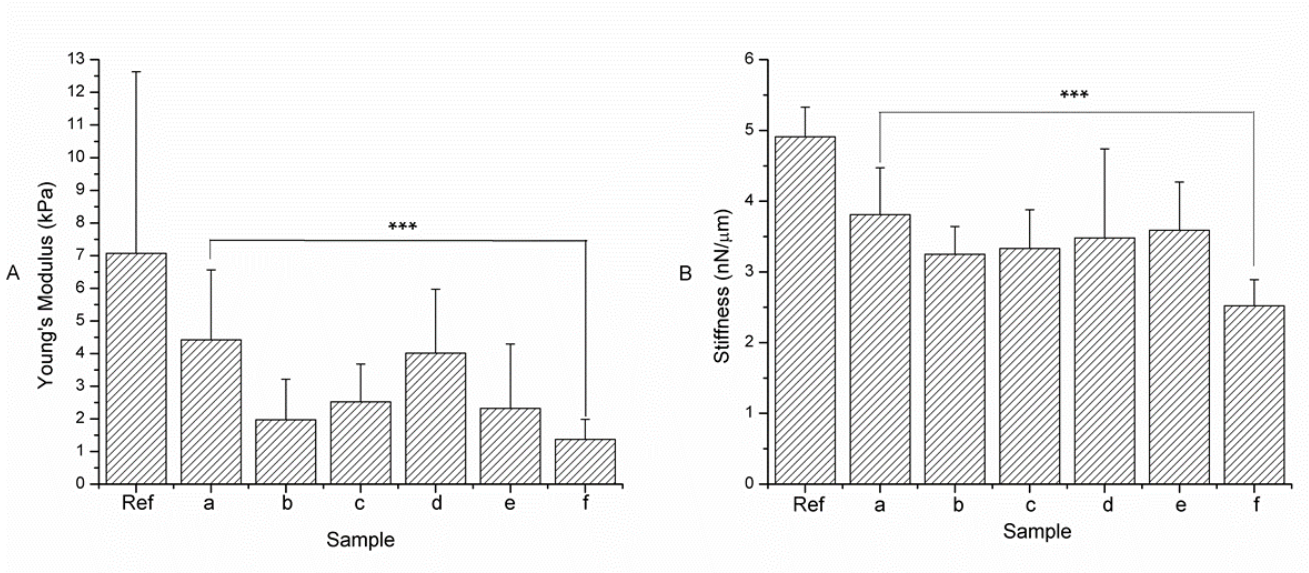


Fig. 6 Histograms of average Young's modulus (A) and stiffness (B) for HeLa cells at different treatments with AMF and MNPs. The treatments showed are a) $Fe_3O_4@SiO_2$, b) $Fe_3O_4@SiO_2$-NH_2, c) 1 h AMF, d) $Fe_3O_4@SiO_2$ 0.5 h AMF, e) $Fe_3O_4@SiO_2$ 1 h AMF and f) $Fe_3O_4@SiO_2$-NH_2 1 h AMF.

The obtained results for Young's modulus showed more drastic changes in values with wider standard deviations compared to the data obtained in stiffness. This behavior can be attributed to the sensitivity of the technique, which could be solved with the acquisition of a greater number of samples to reduce the error. Furthermore, as it is compiled by Deng et al. 2018, although the Young's modulus is one of the most analyzed and reported properties, these results usually fluctuate due to all the variables present through the experiments [37]. This includes the parameters of the measurement equipment, the data processing, as well as the state of the cells and the environmental factors where measurements are performed. The results permit us to contrast with reported studies. The values obtained differ with those reported by Hayashi and Iwata, 2015, where the average value for HeLa cells was 2.48 ± 0.50 kPa, which differed considerably with the 4.42 ± 2.14 kPa obtained in the present study [36]. Our closest values compared with latter research were found for that of AMF-treated cells without MNPs (2.52 ± 1.16 kPa) and AMF with $Fe_3O_4@SiO_2$ (2.32 ± 1.97 kPa).

The histograms obtained from Young's modulus and the stiffness of the reference cells (Fig.A1- Fig.A2) and the exposed cells 1 h AMF with $Fe_3O_4@SiO_2$-NH_2 MNPs (Fig.B1- Fig.B2) are depicted. In the histograms, the decrement in the mean values and in the standard deviation is reflected in narrower curves with left displacements. The optical images of the HeLa cells confirm the existence of the MNPs in contact with cells (Fig.B3), against the untreated cells without MNPs (Fig.A3). The decrease in each of the treated samples indicates that cells become softer and acquire a greater susceptibility to deformation than untreated HeLa cells. Results are consistent with what was reported by Pelling et al. 2009, who described a decrease in the elastic modulus of the cells (5.1 ± 2.9 kPa to 1.6 ± 0.9 kPa) after 120 min treated with staurosporine, due to the cortical actin depolymerization followed by the nucleus collapse [35].

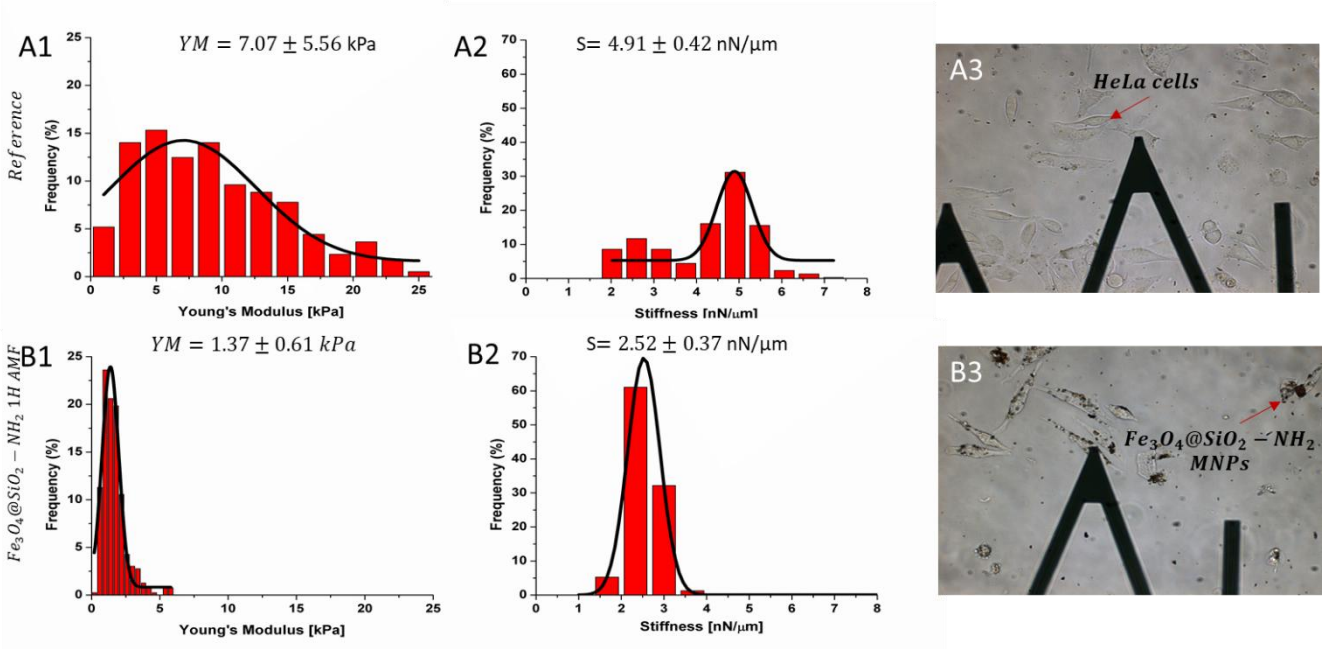


Fig. 7 Histograms of Young's modulus (A1) and stiffness (A2) of the reference cells. Young's modulus had an average value of 7.07 ± 5.56 kPa, while the stiffness had values of 4.91 ± 0.42 nN/µm. A3 corresponds to the optical image of the AFM where the HeLa cells are observed after 24 h of incubation. The histograms in B1 and B2 represent Young's modulus and the stiffness of the treatment with the $Fe_3O_4@SiO_2$-NH_2 MNPs exposed 1 h to the AMF. The average value of Young's module decreased to 1.37 ± 0.61 kPa and the stiffness to 2.52 ± 0.37 nN/µm. In B3 the HeLa cells and the MNPs that are distributed throughout the cells are observed.

4. Conclusions

The synthesized Magnetic Nanoparticles (MNPs) had an effect on the mechanical properties of the HeLa cell membranes. This effect depends primarily on the type of MNPs used. The silica coated MNPs $Fe_3O_4@SiO_2$ had the less effect over the HeLa membranes, with a decrease of 37.48% in Young's modulus and 22.40% in stiffness. On the other hand, functionalized MNPs ($Fe_3O_4@SiO_2$-NH_2) showed to have an effect of 72.13% on Young's modulus and 33.80% on stiffness. The AMF was shown to have significant effects with the cells even without the presence of MNPs, with decreases of 64.35% in Young's modulus and 32.17% in stiffness. However, the result with the appreciable differences was that obtained by applying AMF to $Fe_3O_4@SiO_2$-NH_2 treated cells, since Young's module was reduced 80.62%, while the stiffness value decreased 48.67%. From these results it can be inferred that the silica-coated magnetite nanoparticles are biocompatible since no significant changes were obtained until the application of an Alternating Magnetic Field (AMF). On the contrary, the effect achieved with the functionalized MNPs can be originated due to the amine groups interaction with the cell membranes, which allow the adsorption of the MNPs through charges, or through amide bonds. These could have higher repercussions on the physical properties of the cells. These effects were enhanced with the application of AMF, which indicates that these MNPs have potential for the development of therapies based on heat generation by AMF. Viability tests are required to determine the toxicity of the MNPs, however, this study allowed one to corroborate physical changes in the membrane depending on the type of MNPs, the application of AMF and the exposure time.

Acknowledgements

The authors want to express thanks to CONACYT and Marcos Moshinsky Foundation 2018 for financial support and the PhD scholarship awarded to Juan Carlos Camacho Fernández (Num. X). Also, this work wants to acknowledge the financial support given by SIP-IPN through the project 20195489. Special gratefulness are to Eng. Marcela Guerrero from CINVESTAV-IPN for FT-IR spectrums and Dr Nicolas Cayetano from CNMN-IPN for HR-TEM images.

References

1. Pankhurst, Q.A., et al., Applications of magnetic nanoparticles in biomedicine. Journal of Physics D: Applied Physics, 2003. ***36****(13): p. R167-R181.*

2. Khmara, I., et al., Chitosan-stabilized iron oxide nanoparticles for magnetic resonance imaging. Journal of Magnetism and Magnetic Materials, 2018.

3. Arruebo, M., et al., Magnetic nanoparticles for drug delivery. Nano Today, 2007. ***2****(3): p. 22-32.*

4. Tang, L., J. Casas, and M. Venkataramasubramani, Magnetic Nanoparticle Mediated Enhancement of Localized Surface Plasmon Resonance for Ultrasensitive Bioanalytical Assay in Human Blood Plasma. Analytical Chemistry, 2013. ***85****(3): p. 1431-1439.*

5. Tang, D., R. Yuan, and Y. Chai, Magnetic Core–Shell Fe3O4@Ag Nanoparticles Coated Carbon Paste Interface for Studies of Carcinoembryonic Antigen in Clinical Immunoassay. The Journal of Physical Chemistry B, 2006. ***110****(24): p. 11640-11646.*

6. Silva, A.C., et al., Application of hyperthermia induced by superparamagnetic iron oxide nanoparticles in glioma treatment. International journal of nanomedicine, 2011. ***6****: p. 591-603.*

7. Unni, M., et al., Thermal Decomposition Synthesis of Iron Oxide Nanoparticles with Diminished Magnetic Dead Layer by Controlled Addition of Oxygen. ACS Nano, 2017. ***11****(2): p. 2284-2303.*

8. Zhang, H. and G. Zhu, One-step hydrothermal synthesis of magnetic Fe3O4 nanoparticles immobilized on polyamide fabric. Applied Surface Science, 2012. ***258****(11): p. 4952-4959.*

9. Lemine, O.M., et al., Sol–gel synthesis of 8nm magnetite (Fe3O4) nanoparticles and their magnetic properties. Superlattices and Microstructures, 2012. ***52****(4): p. 793-799.*

10. Ramirez-Nuñez, A.L., et al., In vitro magnetic hyperthermia using polyphenol-coated Fe 3 O 4 @ γ Fe 2 O 3 nanoparticles from Cinnamomun verum and Vanilla planifolia : the concert of green synthesis and therapeutic possibilities. Nanotechnology, 2018. ***29****(7): p. 074001.*

11. Laurent, S., et al., Magnetic Iron Oxide Nanoparticles: Synthesis, Stabilization, Vectorization, Physicochemical Characterizations, and Biological Applications. Chemical Reviews, 2008. ***108****(6): p. 2064-2110.*

12. Dronskowski, R., The Little Maghemite Story: A Classic Functional Material. Advanced Functional Materials, 2001. ***11****(1): p. 27-29.*

13. Wang, L., et al., The study of thermal stability of the SiO2 powders with high specific surface area. Materials Chemistry and Physics, 1999. ***57****(3): p. 260-263.*

14. Schneider, P.M. and W.B. Fowler, Band Structure and Optical Properties of Silicon Dioxide. Physical Review Letters, 1976. ***36****(8): p. 425-428.*

15. Arroyo-Hernández, M., et al., Biofunctionalization of Surfaces of Nanostructured Porous Silicon. Vol. 23. 2003. 697-701.

16. Márquez, F., et al., Preparation of hollow magnetite microspheres and their applications as drugs carriers. Nanoscale Research Letters, 2012. ***7****(1): p. 210.*

17. Wang, J., et al., Two-Phase Synthesis of Monodisperse Silica Nanospheres with Amines or Ammonia Catalyst and Their Controlled Self-Assembly. ACS Applied Materials & Interfaces, 2011. ***3****(5): p. 1538-1544.*

18. Ding, H.L., et al., Fe3O4@SiO2 Core/Shell Nanoparticles: The Silica Coating Regulations with a Single Core for Different Core Sizes and Shell Thicknesses. Chemistry of Materials, 2012. ***24****(23): p. 4572-4580.*

19. Hui, C., et al., Core-shell Fe3O4@SiO2 nanoparticles synthesized with well-dispersed hydrophilic Fe3O4 seeds. Nanoscale, 2011. ***3****(2): p. 701-705.*

20. Morel, A.-L., et al., Sonochemical Approach to the Synthesis of Fe3O4@SiO2 Core−Shell Nanoparticles with Tunable Properties. ACS Nano, 2008. ***2****(5): p. 847-856.*

21. Sperling, R.A. and W.J. Parak, Surface modification, functionalization and bioconjugation of colloidal inorganic nanoparticles. Philosophical Transactions of the Royal Society A: Mathematical, Physical and Engineering Sciences, 2010. ***368****(1915): p. 1333-1383.*

22. Nagano, T., et al., Modifying the Surface of Silica Nanoparticles with Amino or Carboxyl Groups Decreases Their Cytotoxicity to Parenchymal Hepatocytes. Biological and Pharmaceutical Bulletin, 2017. ***40****(5): p. 726-728.*

23. Marzaioli, V., et al., Surface modifications of silica nanoparticles are crucial for their inert versus proinflammatory and immunomodulatory properties. International journal of nanomedicine, 2014. ***9****: p. 2815-2832.*

24. Johannsen, M., et al., Clinical hyperthermia of prostate cancer using magnetic nanoparticles: Presentation of a new interstitial technique. Vol. 21. 2005. 637-47.

25. Kikumori, T., et al., Anti-cancer effect of hyperthermia on breast cancer by magnetite nanoparticle-loaded anti-HER2 immunoliposomes. Breast Cancer Research and Treatment, 2008. ***113****(3): p. 435.*

26. Wang, L., et al., Anticancer effect and feasibility study of hyperthermia treatment of pancreatic cancer using magnetic nanoparticles. Vol. 27. 2011. 719-26.

27. Majeed, J., et al., Enhanced specific absorption rate in silanol functionalized Fe3O4 core–shell nanoparticles: Study of Fe leaching in Fe3O4 and hyperthermia in L929 and HeLa cells. Colloids and Surfaces B: Biointerfaces, 2014. ***122****: p. 396-403.*

28. Hildebrandt, B., et al., The cellular and molecular basis of hyperthermia. Critical Reviews in Oncology/Hematology, 2002. ***43****(1): p. 33-56.*

29. Villanueva, A., et al., Hyperthermia HeLa Cell Treatment with Silica-Coated Manganese Oxide Nanoparticles. The Journal of Physical Chemistry C, 2010. ***114****(5): p. 1976-1981.*

30. Clerc, P., et al., Targeted Magnetic Intra-Lysosomal Hyperthermia produces lysosomal reactive oxygen species and causes Caspase-1 dependent cell death. Journal of Controlled Release, 2018. ***270****: p. 120-134.*

31. Sanchez, C., et al., Targeting a G-Protein-Coupled Receptor Overexpressed in Endocrine Tumors by Magnetic Nanoparticles To Induce Cell Death. ACS Nano, 2014. ***8****(2): p. 1350-1363.*

32. Yallapu, M.M., et al., The roles of cellular nanomechanics in cancer. Medicinal research reviews, 2015. ***35****(1): p. 198-223.*

33. Proa-Coronado, S., et al., Beyond the paradigm of nanomechanical measurements on cells using AFM: an automated methodology to rapidly analyse thousands of cells. Nanoscale Horizons, 2020. ***5****(1): p. 131-138.*

34. Martínez-Rivas, A., et al., WO2019112414 (A1)-2019/06/13. https://patentscope.wipo.int/search/es/detail.jsf?docId=WO2019112414&tab=PCTBIBLIO&maxRec=1000. 2018.

35. Pelling, A.E., et al., Mechanical dynamics of single cells during early apoptosis. Cell Motility, 2009. ***66****(7): p. 409-422.*

36. Hayashi, K. and M. Iwata, Stiffness of cancer cells measured with an AFM indentation method. Journal of the Mechanical Behavior of Biomedical Materials, 2015. ***49****: p. 105-111.*

37. Deng, X., et al., Application of atomic force microscopy in cancer research. Journal of nanobiotechnology, 2018. ***16****(1): p. 102-102.*

*38. Mao, H., et al., Cellular effects of magnetic nanoparticles explored by atomic force microscopy. Biomaterials Science, 2015. **3**(9): p. 1284-1290.*

*39. Hallali, N., et al., Influence on cell death of high frequency motion of magnetic nanoparticles during magnetic hyperthermia experiments. Applied Physics Letters, 2016. **109**(3): p. 032402.*

*40. Daou, T.J., et al., Hydrothermal Synthesis of Monodisperse Magnetite Nanoparticles. Chemistry of Materials, 2006. **18**(18): p. 4399-4404.*

*41. Sahoo, Y., et al., Alkyl Phosphonate/Phosphate Coating on Magnetite Nanoparticles: A Comparison with Fatty Acids. Langmuir, 2001. **17**(25): p. 7907-7911.*

*42. Silva, V.A.J., et al., Synthesis and characterization of Fe3O4 nanoparticles coated with fucan polysaccharides. Journal of Magnetism and Magnetic Materials, 2013. **343**: p. 138-143.*

*43. Zhan, S., et al., Efficient removal of pathogenic bacteria and viruses by multifunctional amine-modified magnetic nanoparticles. Journal of Hazardous Materials, 2014. **274**: p. 115-123.*

*44. Girginova, P.I., et al., Silica coated magnetite particles for magnetic removal of Hg2+ from water. Journal of Colloid and Interface Science, 2010. **345**(2): p. 234-240.*

*45. Rahman, I.A., M. Jafarzadeh, and C.S. Sipaut, Synthesis of organo-functionalized nanosilica via a co-condensation modification using γ-aminopropyltriethoxysilane (APTES). Ceramics International, 2009. **35**(5): p. 1883-1888.*

*46. Bruce, I.J. and T. Sen, Surface Modification of Magnetic Nanoparticles with Alkoxysilanes and Their Application in Magnetic Bioseparations. Langmuir, 2005. **21**(15): p. 7029-7035.*

*47. Zhang, S., et al., Thiol modified Fe3O4@SiO2 as a robust, high effective, and recycling magnetic sorbent for mercury removal. Chemical Engineering Journal, 2013. **226**: p. 30-38.*

*48. Yang, L., et al., Modification and Characterization of Fe3O4 Nanoparticles for Use in Adsorption of Alkaloids. Molecules, 2018. **23**(3): p. 562.*